AGU PUBLICATIONS

JGR

Journal of Geophysical Research: Oceans

RESEARCH ARTICLE

10.1002/2015JC011375

Key Points:

- The Atlantic water inflow and eddy at the Fram Strait are simulated by high-resolution ocean model
- The contribution of oceanic eddy to the heat flux is examined
- Interannual variability of heat flux is explained by the variability of wind

Correspondence to:
T. Kawasaki,
kawasaki@aori.u-tokyo.ac.jp

Citation:
Kawasaki, T., and H. Hasumi (2016), The inflow of Atlantic water at the Fram Strait and its interannual variability, *J. Geophys. Res. Oceans*, *121*, 502–519, doi:10.1002/2015JC011375.

Received 13 OCT 2015
Accepted 4 DEC 2015
Accepted article online 13 DEC 2015
Published online 14 JAN 2016

The inflow of Atlantic water at the Fram Strait and its interannual variability

Takao Kawasaki[1,2] and Hiroyasu Hasumi[2]

[1]Arctic Environment Research Center, National Institute of Polar Research, Tachikawa, Japan, [2]Atmosphere and Ocean Research Institute, University of Tokyo, Kashiwa, Japan

Abstract The heat influx of the Atlantic water and its interannual variability through the Fram Strait toward the Arctic Ocean are examined by using a realistically configured ice-ocean general circulation model. The modeled routes of the Atlantic water and high eddy activity around the Fram Strait are consistent with many observations. Two-thirds of the heat transported by the Atlantic water passing through the Fram Strait (78°N) is lost by the westward transport and the sea surface cooling, and the other one-third is injected to the Arctic Ocean. The contribution of oceanic eddy to the westward heat transport is 5% of that of mean current. The variability of sea level pressure anomaly centered at the Nordic Seas explains the interannual variability of the heat passing through the Fram Strait, transported westward, and cooled at the sea surface in the north of the Fram Strait. The interannual variabilities of these heat fluxes have significant correlations with the NAO. The interannual variability of heat transported by the Atlantic water and entering the Arctic Ocean is caused by the variability of the Siberian high.

1. Introduction

Satellite observations revealed that the area of the summer Arctic sea ice has steadily decreased in recent decades [*Comiso et al.*, 2008]. Submarine-observed data further indicate that its thickness has also been declining [*Rothrock et al.*, 1999, 2008]. A lot of attention is paid to possible influences of the rapid loss of the Arctic sea ice on the climate system [*Serreze et al.*, 2007; *Screen and Simmonds*, 2010]. The changes in Arctic sea ice also have a significant socioeconomic impact through maritime logistics, since the decrease of sea ice is expected to extend the available period of the Arctic ship route. Interannual variability of the Arctic sea ice is controlled not only by heating or cooling by the atmosphere but also by the heat flux from the ocean underneath. Cold low salinity water originated in the river runoff covers the sea surface in the Arctic Ocean. Warm Pacific Water passing through the Bering Strait lies just below it, and a change of its behavior caused the recent drastic decline of Arctic sea ice [*Shimada et al.*, 2006]. Below Pacific Water, the Atlantic Layer Water is found (~150–400 m depth), which is originated from the Atlantic water entering through the Fram Strait and contains a larger amount of heat than Pacific Water [*Aagaard and Greisman*, 1975; *Lique*, 2015]. It melts the Arctic sea ice through the significant upward heat flux by the enhanced vertical mixing over the rough topography [*Rippeth et al.*, 2015] and double diffusion [*Polyakov et al.*, 2012] along the Barents and Laptev Slopes.

Walczowski and Piechura [2006] showed that the heat content of the Atlantic water, which is transported by the West Spitsbergen Current (WSC), increased to the south of 79°N during the 2001–2005 period based on the conductivity and temperature depth (CTD) profiler observations. Mooring observation data indicated warming of the Atlantic water at the Fram Strait (79°N) [*Schauer et al.*, 2004, 2008]. An increase of temperature, by 0.8°C from February to August 2004, is observed for Atlantic Layer Water flowing along the Eurasian continental slope by mooring at the north of the Laptev Sea [*Dmitrenko et al.*, 2008]. Warming of Atlantic Layer Water is observed also in the Makarov Basin in the first half of the 1990s [*Aagaard et al.*, 1996]. Several observations reported that Atlantic Layer Water had been warming in the 1990s and 2000s in the Canadian Basin [*Carmack et al.*, 1995; *Shimada et al.*, 2004]. As describe above, many observations have implied that the warming of the Atlantic water transported through the Fram Strait causes the warming of Atlantic Layer Water. The warming of Atlantic Layer Water could contribute to drastic reduction of the Arctic sea ice in the future [*Polyakov et al.*, 2010; *Lique*, 2015].

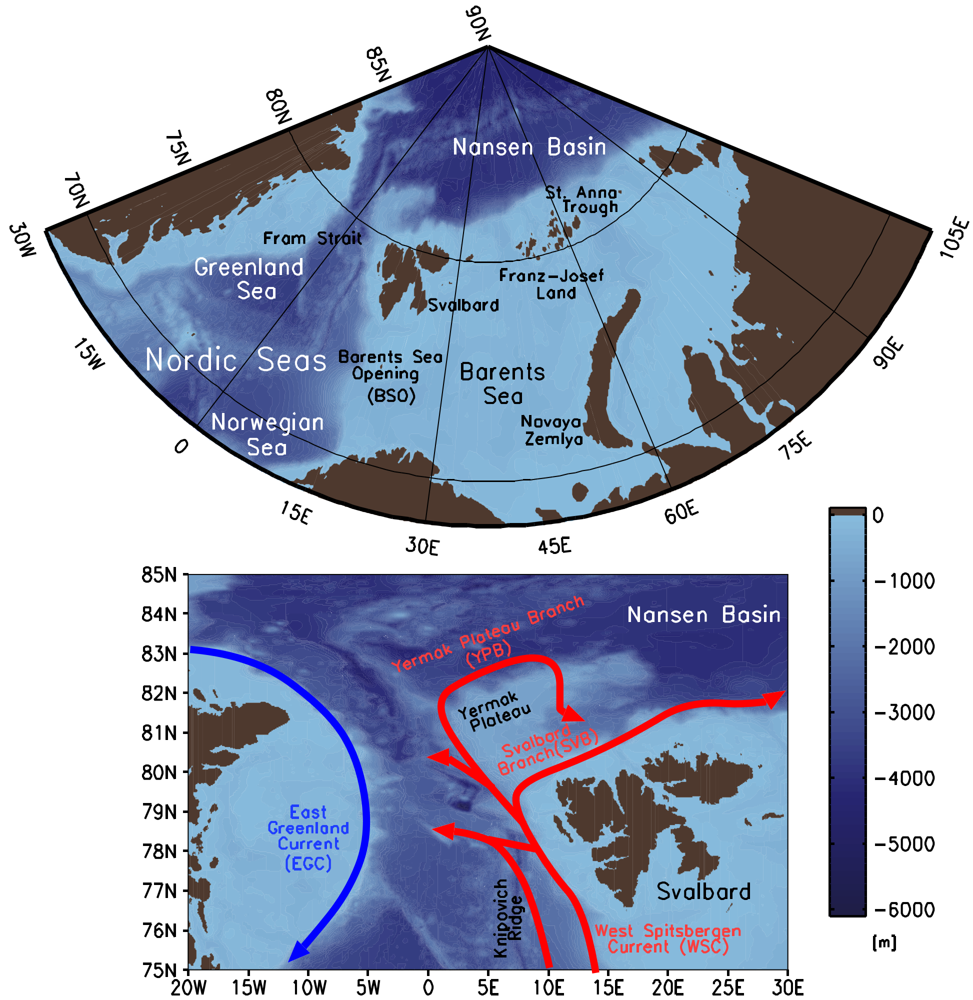

Figure 1. (top) The bathymetry of the Nordic Seas, the Barents Sea, and the Nansen Basin. (bottom) A schematic for the circulation of warm/salty Atlantic water (red arrow) and cold/fresh East Greenland Current (blue arrow) around the Fram Strait.

For monitoring the water passing through the Fram Strait, many moorings have been deployed and repeated CTD observations have been conducted along 79°N [*Schauer et al*., 2008; *Beszczynska-Möller et al*., 2012]. On the other hand, the ocean circulation and its variability to the north of 79°N have not been described so clearly as those to the south due to the observational difficulty caused by sea ice. The Yermak Plateau Branch (YPB), which is the boundary current along the margin of the Yermak Plateau, and Svalbard Branch (SVB), which flows along the northern continental slope of the Svalbard, bifurcate from the WSC at ~80°N (Figure 1) [*Aagaard et al*., 1987]. *Cokelet et al*. [2008] exhibited that the temperature of the Atlantic water decreased by 0.25°C/100 km toward the downstream along the SVB by the CTD observation in fall 2001. This implies that there are some mechanisms which function to reduce the heat transported by the Atlantic water into the Arctic Ocean.

Aagaard et al. [1987] suggested that a part of the YPB returns to the Atlantic Ocean as a returning current at the north of 80°N and the remaining part enters the Arctic Ocean. Several returning currents are observed along oceanic bottom fracture zones [*Quadfasel et al*., 1987; *Bourke et al*., 1988]. An observation conducted in 2002 around the East Greenland Current (EGC) implied that the Atlantic water transported by the YPB to the north of 81°N flows along the Yermak Plateau and into the Arctic Ocean without returning to the Greenland Sea [*Rudels et al*., 2005].

A tortuous or vortical structure of sea-ice margin observed by satellite and aircraft suggests that the warm Atlantic water is transported by mesoscale eddies and melts the sea ice on the eastern side of Greenland [*Johannessen et al*., 1987, 2003]. A simplified model showed that 1.4 TW (1 TW = 10^{12} W) of heat is drawn away from the WSC by meandering and eddies formed as a result of barotropic instability [*Teigen et al*., 2010].

Although some observational studies quantified the effect of eddies and returning currents on the inflow of the Atlantic water to the Arctic Ocean, the spatial and temporal sparseness of such observations prohibits us from adequately validate those estimates. A realistically configured ocean general circulation model could be of help in this regard. However, it is difficult for low-resolution models to explicitly simulate the eddy activity around the Fram Strait, because the deformation radius is small due to high latitude. The northward transport of the Atlantic water by the narrow WSC, whose width is several tens of kilometers, is not explicitly reproduced in low-resolution models. *Maslowski et al*. [2004] utilized a pan-Arctic high-resolution (horizontal grid size is $\sim$9 km) ocean model and demonstrated the comparable contribution of Atlantic water inflow by the Fram Strait and Barents Sea branches. *Aksenov et al*. [2010] also studied on the mass, heat and salt flux in a similar resolution ocean model and showed the larger contribution of the Fram Strait branch to heat flux to the Arctic Ocean than that of Barents Sea branch. Since horizontal grid sizes of state-of-the-art high-resolution ice-ocean models are $\sim$8–9 km, they cannot completely resolve the mesoscale eddy activity around the Fram Strait [*Maslowski et al*., 2004; *Aksenov et al*., 2010, 2011]. Moreover, those previous modeling studies have not shown the factors of interannual variability of heat flux at the Fram Strait. In this study, we try to reproduce the Atlantic water inflow (the WSC and eddy activity) to the Arctic Ocean as realistically as possible by using an ice-ocean model with high-horizontal resolution around the Fram Strait. Then, we examine the heat transport to the Arctic Ocean by the Atlantic water passing through the Fram Strait with focusing on: (1) the amount of heat removed by eddies, returning currents, and sea surface cooling, and (2) factors controlling the interannual variability of heat transport at the north of the Fram Strait (79°N).

2. Model Description and Experimental Design

The ice-ocean general circulation model employed in this study is COCO version 4.5 [*Hasumi*, 2006]. The model incorporates a second-order moments conserving scheme for tracer advection [*Prather*, 1986]. A turbulence closure scheme based on a generic length-scale equation [*Umlauf and Burchard*, 2003] is applied for diagnosing vertical viscosity and diffusivity. The effect of submesoscale eddy is also parameterized [*Fox-Kemper et al*., 2008; *Fox-Kemper and Ferrari*, 2008]. Background vertical diffusivity is 1.0×10^{-6} m^2 s^{-1}, which is quite smaller than that typically used in the other basins, based on a microstructure measurement across the Arctic Ocean [*Rainville and Winsor*, 2008]. The horizontal biharmonic friction with Smagorinsky-like viscosity is utilized, where the value of controlling parameter is set to 3 [*Griffies and Hallberg*, 2000].

The sea-ice component includes one layer thermodynamics [*Bitz and Lipscomb*, 1999] and elastic viscous plastic dynamics of *Hunke and Dukowicz* [1997] with five category ice thickness [*Bitz et al*., 2001]. The thresholds of ice thickness categories are 0.2, 0.6, 1.4, 3.0, and 6.0 m. The number of categories and their range of sea-ice thickness are selected based on a previous modeling study [*Komuro and Suzuki*, 2013]. A linear remapping scheme [*Lipscomb*, 2001] is used to calculate thermodynamic transfers of ice and snow between the categories.

The model domain is global. As the Rossby's deformation radius is $\sim$10 km around the Fram Strait [*Walczowski*, 2013], effects of mesoscale eddies cannot be explicitly represented unless the horizontal grid size is significantly smaller than 10 km. As in the study by *Kawasaki and Hasumi* [2014], special high resolution is applied to the region of interest by placing the poles of the general curvilinear horizontal coordinates close to the region, on northern Greenland and Scandinavian Peninsula. The horizontal resolution is eddy resolving (2–3 km) in the Fram Strait and the Barents Sea Opening (BSO), and is eddy permitting (3–10 km) around the Nordic Seas, the Barents Sea, and the Nansen Basin (Figure 2). The bathymetry is constructed from a 2 min topography data set (ETOPO2) [*National Geophysical Data Center, National Oceanic and Atmospheric Administration*]. There are 45 vertical levels, and the grid spacing varies from 5 (top) to 500 m (bottom: 6370 m depth). A horizontally low-resolution experiment is also conducted for comparison, where the only difference from the model described above is that the numbers of horizontal grid are reduced 1/8 in both directions.

The model is initiated by climatological temperature and salinity (PHC 3.0) [*Steele et al*., 2001] with no oceanic motion and sea ice. The sea surface heat, freshwater, and momentum fluxes are calculated using the corrected interannual forcing data sets for common ocean-ice reference experiments (CORE) [*Large and Yeager*, 2009]. The integrated period is from 1980 to 2010. The first 10 years (1980–1990) is for spin-up of

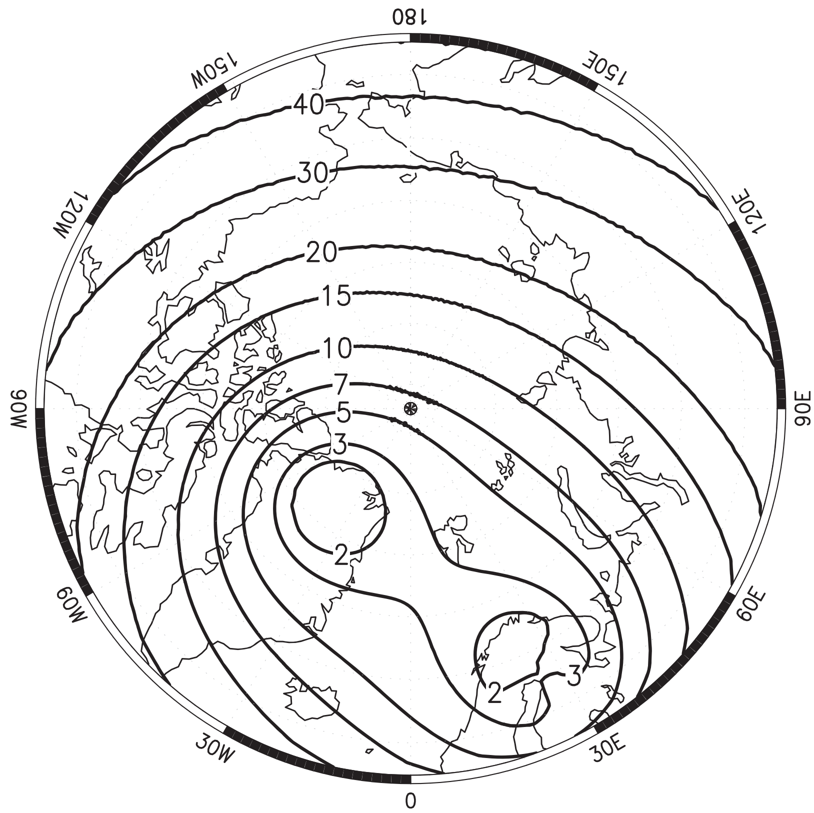

Figure 2. Horizontal grid size of model (km).

sea-ice distribution and mean circulation in and around the Arctic Ocean. The temperature and salinity are restored to observed monthly climatology [*Steele et al.*, 2001] with a damping time scale of 10 days below 120 m and at all depths, respectively, in this period. After the 10th model year (1990–2010), such restoring is not employed. Since it takes time for eddies to develop, only the last 17 years of the integrated period (1993–2010) are examined in this study.

3. Results

3.1. Routes of Inflow of the Atlantic Water Through the Fram Strait and Barents Sea

The modeled temperature and salinity around the Fram Strait and the Barents Sea averaged in the shallow layer (0–300 m depth) and for 1993–2010 are displayed in Figure 3. The warm, salty Atlantic water is transported northward by the Norwegian Atlantic Current in the Norwegian Sea. A part of the Norwegian Atlantic Current flows into the Barents Sea through the BSO and the rest flows into the Nansen Basin through the Fram Strait. The Atlantic water entering the Barents Sea flows northeastward along several routes constrained by the bathymetric structure on the shelf. This water reaches the Nansen Basin by passing between Franz-Josef Land and Novaya Zemlya and through the St. Anna Trough. These routes of the Atlantic water through the Barents Sea are consistent with an observational study [*Schauer et al.*, 2002] and a previous modeling study [*Maslowski et al.*, 2004]. The Arctic Shelf Break Branch is also found in the distribution of salinity in our model (Figure 3b). This branch is suggested by a previous modeling study [*Aksenov et al.*, 2011] to pass through the strait between the Svalbard and Franz-Josef Land with a smaller amount of transport than that through the St. Anna Trough. The net volume transports through the Fram Strait, the WSC, and the BSO are shown in Table 1. All simulated volume transports are slightly larger than observed. The net southward volume transport at the Fram Strait is comparable with the net eastward volume transport at the BSO, which is consistent with observations.

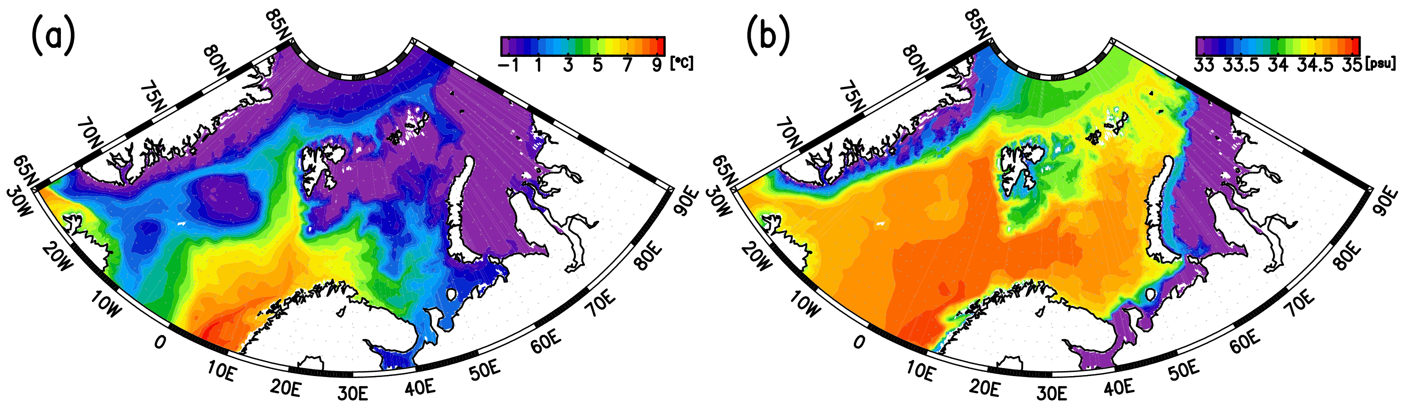

Figure 3. Distribution of (a) potential temperature and (b) salinity averaged in the shallow layer (over 0–300 m depth) and for 1993–2010.

The 17 year mean heat transports at the Fram Strait and the BSO is 58 and 88 TW, respectively, when −0.1°C is chosen as the reference temperature for the sake of comparison with previous observed estimates. In comparison to a mooring observation (16–41TW in 1997–1999 and 40–50TW in 2004–2006) [*Schauer et al*., 2004, 2008], it is slightly higher at the Fram Strait. Since *Schauer et al*. [2008] estimated that the maximal error of heat flux at the Fram Strait is ±6 TW associated with the spatial interpolation of mooring data, it is likely that the heat flux is overestimated in our model. This overestimation may be attributed to a high-temperature bias of the Atlantic water as described hereinafter. However, the conclusion of this study (relative importance of heat loss by eddies, returning currents, and sea surface cooling; and the factor controlling interannual variability of heat flux) are unaffected by this bias.

The heat flux at the BSO is in the range of estimates by a mooring observation (73 TW) [*Smedsrud et al*., 2010] and an inverse model (103 TW) [*Tsubouchi et al*., 2012]. As the heat flux into the Nansen Basin through the St. Anna Trough is −12 TW (the negative value means that the temperature of passing water is less than −0.1°C), it is obvious that the Atlantic water flowing through the Fram Strait has larger contribution to heat supply to the Nansen Basin than that through the Barents Sea.

The temperature of the Atlantic water entering the Nansen Basin through the Barents Sea and St. Anna Trough is low because of the strong sea surface cooling on the way flowing northeastward on the shelf (Figure 3a). On the other hand, the Atlantic water flowing through the Fram Strait toward the Nansen Basin retains a high-temperature property. As a consequence, the Atlantic water transported through the Fram Strait provides the Arctic Ocean with a larger amount of heat than that through the Barents Sea.

Mean meridional velocity and potential temperature distributions at the Fram Strait (along 79°N) between 2002 and 2008 are shown in Figures 4a and 4b. This period is selected for comparison with an observational study (Figure 5) [*Beszczynska-Möller et al*., 2012]. The warm Atlantic water is transported northward by the WSC at the eastern Fram Strait (on the side of the Svalbard). On the other hand, the cold Polar Water is transported southward by the EGC at the western Fram Strait (on the side of the Greenland). This qualitative feature of currents is consistent with many observations (Figure 5) [e.g., *Schauer et al*., 2004, 2008]. The simulated width of the WSC is 40–50 km and larger than that estimated by observations (∼20–30 km; Figure 5b). Although the observed WSC is located around 8–9°E and barotropic, the simulated WSC is in a region westward (6–7°E) and its barotropic component is weak (Figures 4b and 5b). Similar bias was found in a previous modeling study [*Aksenov et al*., 2011, Figures 2d and 2h]. A small core of northward current around 8–9°E, which was not seen in *Aksenov et al*. [2011], is simulated in our model. This small but significant improvement is presumed to be caused by the fact that the horizontal grid size is 2–3 km in our model, whereas that is 8–9 km in

Table 1. Net Volume Transport at the Fram Strait, the WSC, and Barents Sea Opening (BSO) in Our Model and Observations (Sv; 1 Sv = 106 m^3 s^{-1})

		Model	Observation	Period	Reference
Fram	(Southward)	2.8	2.0	1997–2006	*Schauer et al.* [2008]
WSC	(Northward)	7.1	6.6	1997–2010	*Beszczynska-Möller et al.* [2012]
BSO	(Eastward)	2.4	2.0 (2.6)[a]	1997–2007	*Smedsrud et al.* [2010]

[a]The BSO net volume transport of 2.0 Sv is calculated based on the Norwegian Coastal Current (NCC) of 1.2 Sv (see the text in *Smedsrud et al*. [2010], for detail). However, since the NCC of 1.8 Sv is estimated by *Skagseth et al*. [2011], we should employ the updated value (2.6 Sv) when we calculated the total volume transport at the BSO.

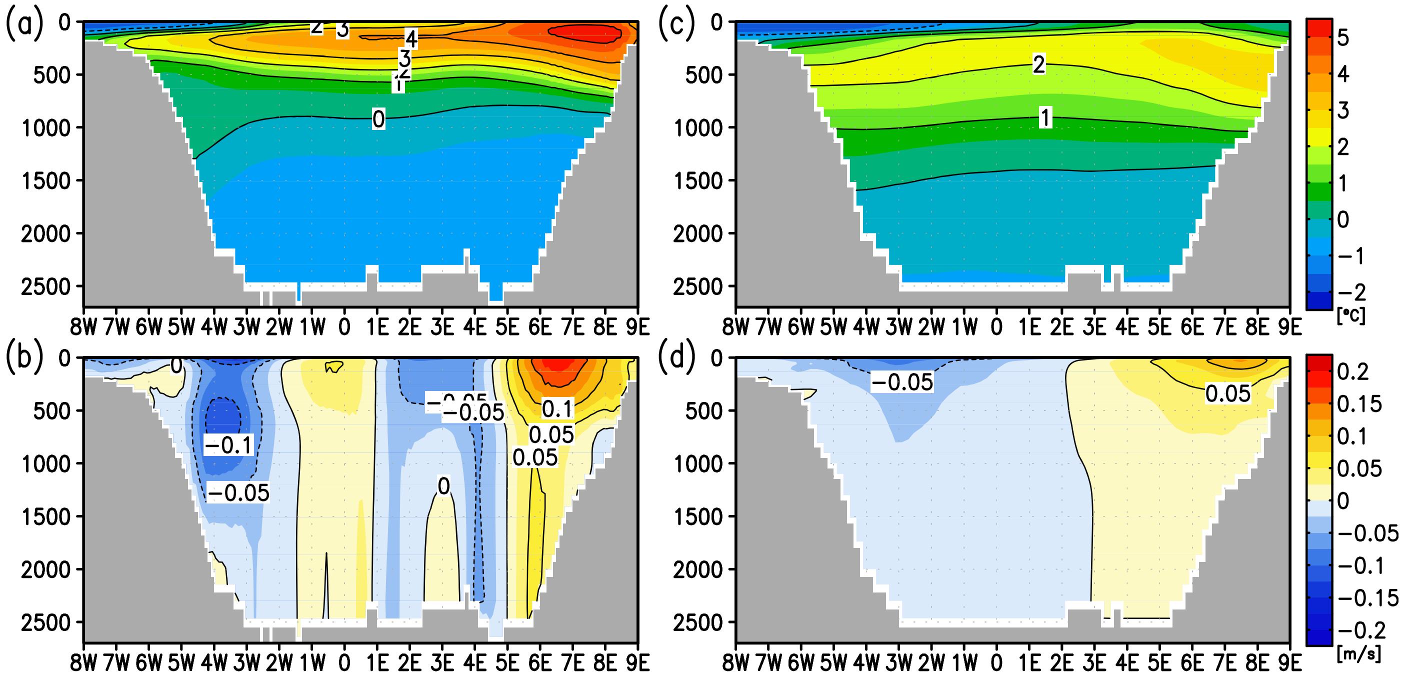

Figure 4. Distributions across the Fram Strait (79°N) of (a) temperature and (b) meridional velocity averaged for 2002–2008 (in °C and m s^{-1}). (c and d) Same as (a and b) but for in the low-resolution model.

the previous study [*Aksenov et al.*, 2011]. The simulated potential temperature of WSC core (~5°C; Figure 4a) is higher than observational estimate (~4°C; Figure 5a). As described in the previous section, the overestimate of heat flux is caused by this high-temperature bias. This high-temperature bias does not have a large effect on the heat flux analysis described in next section, because the difference of simulated and observed sea surface heat flux is quite small as follows. Generally, the heat flux at the sea surface is approximately proportional to the difference of oceanic and air temperature. Then, the error of heat flux is estimated to be ~5% based on the typical winter air temperature around the Fram Strait (~−15°C in 10°W–10°E, 76–82°N, 1990–2010).

To show the improvement by higher horizontal resolution, we conducted a horizontally low-resolution experiment. Since the horizontal grid size is ~20 km around the Fram Strait, mesoscale eddies are not resolved in the low-resolution model. The maximum velocity of WSC (0.1 m s^{-1}; Figure 4d) is the half of that in high-resolution model and mooring observational estimate (~0.2 m s^{-1}; Figure 5b). The sea surface core of EGC is also weaker (0.05 m s^{-1}; Figure 4d) than that in the high-resolution model and observation (0.1 m s^{-1}; Figure 5b). While the other currents are found between the WSC and EGC in observation and high-resolution model, such fine current structure is not reproduced in the low-resolution model (Figure 5b). The temperature in WSC core is too low (~2.5°C) and lies at 300–500 m depth in the low-resolution model, because the WSC is too weak to reach this section before near surface water is completely cooled (Figure 5a).

3.2. Mean Currents and Eddy Activities Around the Fram Strait

The 17 year mean potential temperature and horizontal velocity at 150 m depth, where the maximum of modeled WSC temperature is located, around the Fram Strait is shown in Figures 6a and 6b. A part of the Atlantic water is transported westward along the Knipovich Ridge and Greenland-Spitsbergen Sill between 78°N and 79°N (Knipovich Branch) and joins the EGC. That is, this part returns to the Greenland Sea. This result is similar to a previous modeling study [*Aksenov et al.*, 2010].

The WSC bifurcates into the SVB and YPB to the north of 79°N in our model. The simulated SVB flows eastward along the northern continental slope of the Svalbard and continues to the shelf boundary current in the Nansen Basin. The modeled YPB turns clockwise along the Yermak Plateau and joins the SVB. This current was observed by *Saloranta and Haugan* [2001] and *Rudels et al.* [2000].

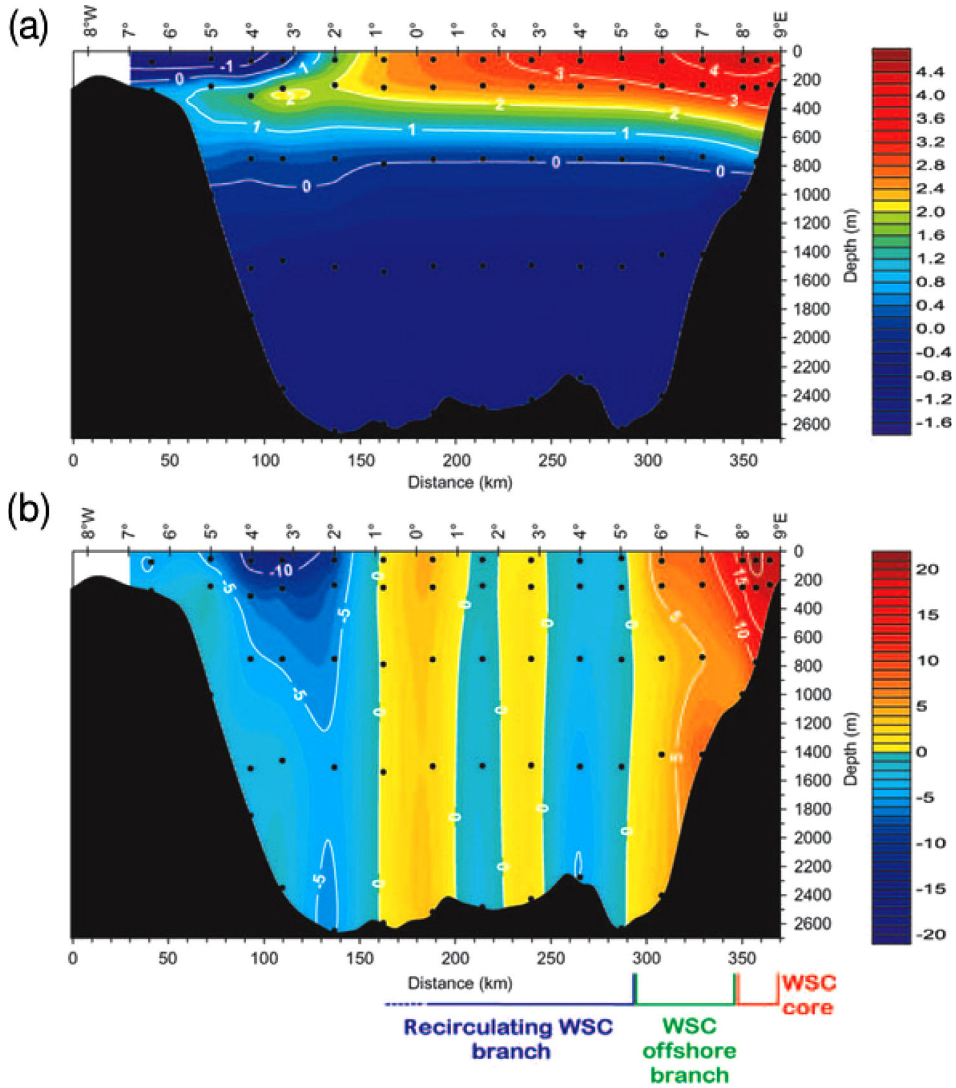

Figure 5. Observed distributions across the Fram Strait (~79°N) of (a) temperature and (b) meridional (cross section) velocity averaged for 2002–2008 (in °C and cm s^{-1}) from *Beszczynska-Möller et al.* [2012].

The modeled northward flowing YPB passes the region of high eddy activity and is more blurred than the SVB. The bifurcation of westward current along the Molloy Fracture Zone from the YPB between 80°N and 81°N is simulated. This westward transport of the Atlantic water was observed by *Quadfasel et al.* [1987]. The most part of the westward-transported Atlantic water joins the EGC and returns to the Greenland Sea in our model.

The simulated southward flow from the Nansen Basin, located around 0–15°E, 84°N, is a part of the anti-clockwise boundary current in the Nansen Basin and transports the cold Polar Water. A major part of it flows eastward and joins the YPB and SVB, although a small part of the southward flow joins the EGC and is exported to the Greenland Sea in our simulation.

Eddy activity can be explicitly reproduced in our model because of the significantly smaller horizontal grid size (2–3 km) than the deformation radius around the Fram Strait (9–11 km) [*Walczowski*, 2013]. Figure 6c depicts the five-daily (4–8 August 2003) mean sea surface temperature (SST) and sea-ice concentration around the Fram Strait. The warm water transported by the WSC is found in the eastern side, and the sea ice transported by the EGC from the Arctic Ocean is found in the western side. Eddies are found in the center of the Fram Strait, and they transport the warm Atlantic water, which reaches there by the WSC, westward. As a consequence of the melting of sea ice induced by the westward-transported warm water by

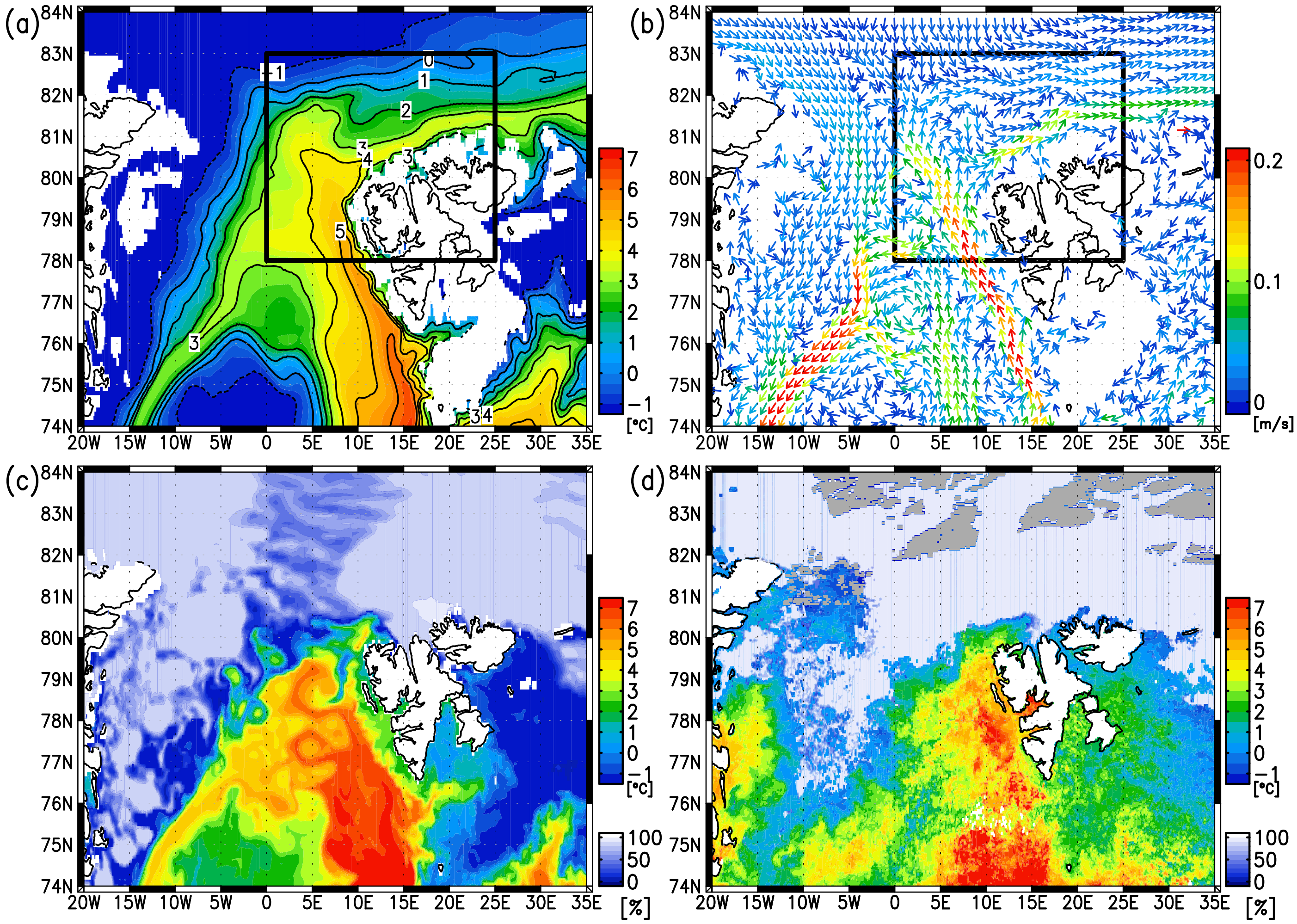

Figure 6. Distribution of 17 year mean (a) potential temperature (°C) and (b) horizontal velocity (m s^{-1}) at 150 m depth around the Fram Strait. Color of vector indicates scalar velocity, and vector is drawn every 1.0° and 0.3° in zonal and meridional, respectively. (c) Distribution of five-daily mean sea surface temperature (SST; °C) and sea-ice concentration (%) for 4–8 August 2003. (d) Similar to (c) but observation and nine-daily mean (2–10 August 2003) for sea-ice concentration. The longer period mean is utilized to decrease the undefined data for sea-ice concentration. The SST [*NASA Goddard Space Flight Center*, 2014] and sea-ice concentration [*Hall and Riggs*, 2015] are based on the high-resolution satellite (MODIS) observation data.

eddies, the shape of sea-ice margin is meandering. This structure is captured by satellite data (Figure 6d). This eddy-induced westward transport of the warm water causes a heat loss of the Atlantic water flowing toward the Nansen Basin.

3.3. Interannual Variability of Temperature and Volume Transport at the Fram Strait

The time series of temperature at the Fram Strait (along 79°N) is shown in Figure 7. The warm water at the eastern end is the Atlantic water transported by the WSC, and the cold water at the western end is the Polar Water transported by the EGC. The warming of the Atlantic water transported by the WSC from the late 1990s to the mid-2000s [*Schauer et al*., 2008, 1°C/8 years] is well reproduced. The model has a slightly warm bias related to the overestimate of heat flux at the Fram Strait as described previously. The seasonal variability of the Atlantic water temperature, such as the peak of WSC temperature in autumn, is also well reproduced in this region.

We calculated heat transport at the Fram Strait in previous section to compare with observational studies. However, this estimated heat transport depends on the selection of reference temperature when the net volume transport is not zero at the section. *Schauer and Beszczynska-Möller* [2009] avoided this problem for WSC heat flux by using the "stream tube concept," which defines the minimum temperatures of the WSC water and its returning current water such that the net volume flux of them becomes zero. Here we also employ this method for calculation of WSC heat flux at the Fram Strait (~79°N). Figures 8a and 8b show the

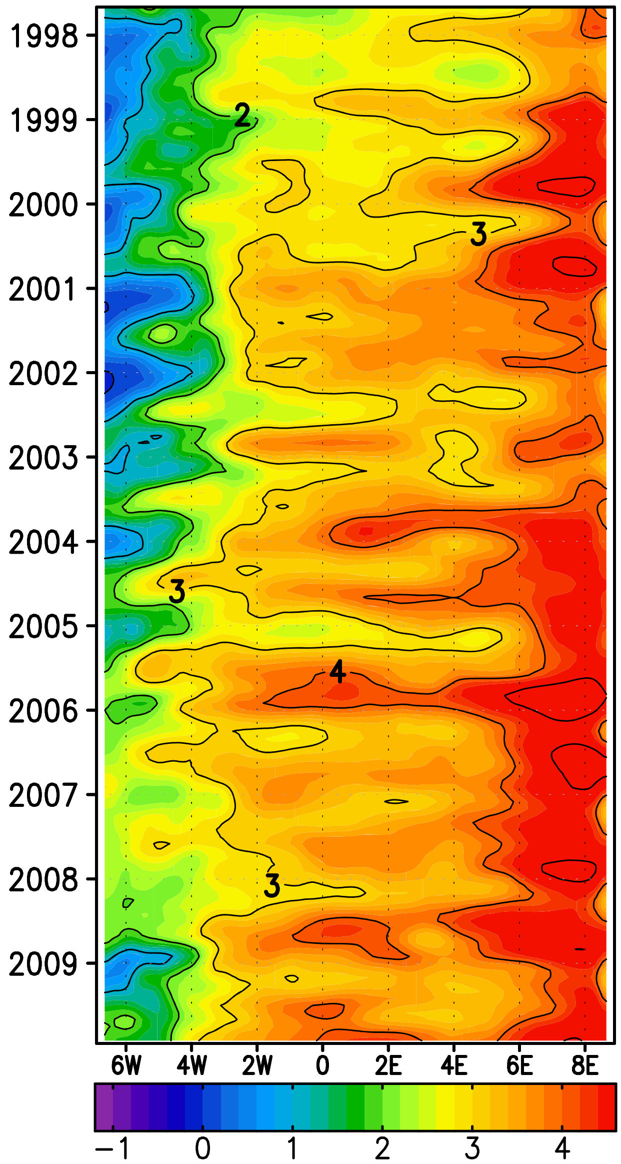

Figure 7. Hovmöller diagram of temperature distribution across the Fram Strait (79°N) at 250 m depth from 1997 to 2010.

time series of heat transport and temperatures of inflow and outflow at the Fram Strait. These figures are similar to Figures 3a and 4 in *Schauer and Beszczynska-Möller* [2009] except for the minimum temperature of the WSC (here we select 2°C instead of 1°C). Although the increase of annual running mean heat flux from 1997/1998 winter to 1999 (observation: 26–36 TW) is overestimated (model: 32–58 TW), the upward trend is well reproduced in our model (Figure 8a). The downward trend of heat flux from 2000 to 2002 is also well reproduced in our model. The simulated increment of heat flux from early to mid-2000s is 36 TW and one-and-a-half times as large as that observed (24 TW).

The interannual variability of simulated WSC temperature (red line in Figure 8b) is consistent with observation [*Schauer and Beszczynska-Möller*, 2009, Figure 4]. Since this interannual variability of temperature is related to that of heat flux, the largest heat flux and highest temperature are found in 2006 in our model. However, the observed largest heat flux is not found in 2006. *Schauer and Beszczynska-Möller* [2009] pointed out that the asynchronicity between the largest heat flux and the highest temperature is caused by the continual warming of outflow from 2004 to 2006 [1°C/2 years; blue line in *Schauer and Beszczynska-Möller*, 2009, Figure 4]. As the simulated warming of outflow in 2004–2006 is not large ($<$0.1°C; Figure 8b), the peak of heat flux is inconsistent with observation. The increases of heat flux in 1998–1999 and 2002–mid-2000s and the decreases in 2000–2002 and after mid-2000s are consistent with observation (Figure 8a). The annual running means of heat flux at the Fram Strait and volume transport of WSC have strong synchronicity ($r > 0.9$) in our model (Figures 8a and 8c). The simulated interannual variability of volume transport of WSC is generally similar to observed one [*Beszczynska-Möller et al.*, 2012, Figure 6c] except for the simulated largest volume flux in 2006.

As stated above, the simulated routes of the Atlantic water inflow, temperature, and volume transport of the WSC, associated heat fluxes, and their interannual variabilities are consistent with observed features. Thus, it is meaningful to investigate the Atlantic water inflow at the Fram Strait by examining the result of our model.

3.4. Heat Flux Around The Fram Strait

In this section, we quantitatively examine the volume and heat fluxes to the north of the Fram Strait (78°N). The heat flux is given as,

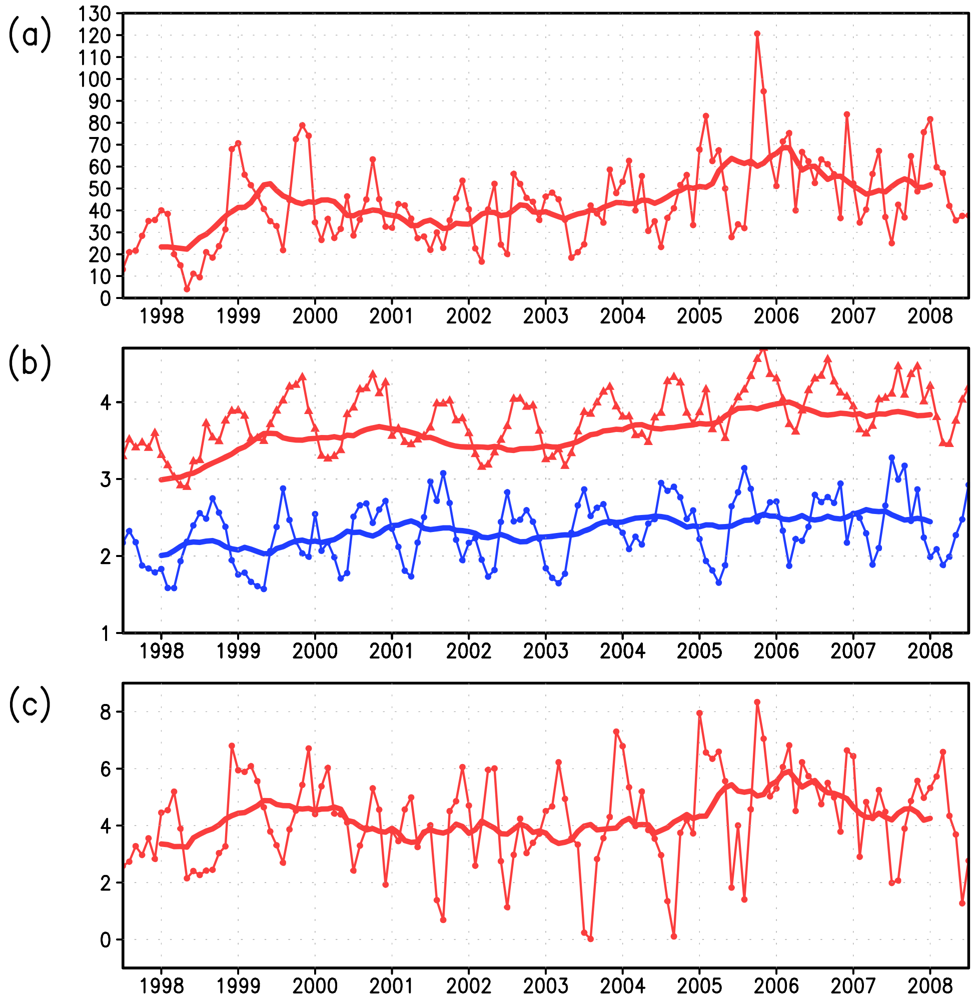

Figure 8. (a) Time series of heat transport to the Arctic Ocean through the WSC water (warmer than 2°C) at the Fram Strait (~79°N). (b) The temperature of northward flow of water warmer than 2°C (red) and southward flow of water warmer than a minimum temperature of outflow (t_{out}) at the Fram Strait. The detail methods of calculation of heat flux and t_{out} are described in the original paper [*Schauer and Beszczynska-Möller*, 2009]. Although 1°C is selected for the definition of the WSC water in *Schauer and Beszczynska-Möller* [2009], here we use 2°C because of the warm bias by 1°C in our model. (c) Volume transport of the WSC (water warmer than 2°C and between 4°E and 9°E). This figure is similar to Figure 6c in *Beszczynska-Möller et al.* [2012], but the western boundary of the WSC is different by 1° (5–9°E in the original paper) because of the location bias of the modeled WSC. Thin and thick lines indicate monthly and annual-running mean, respectively.

$$\int_A c_p \rho (\theta - \theta_{ref}) v \mathrm{d}A, \tag{1}$$

where A is any cross-section surface, c_p is the specific heat of seawater, ρ is density of seawater, θ is potential temperature, and v is cross-section velocity. θ_{ref} is a reference potential temperature, and we choose -1.8°C, approximately the freezing point of seawater, here. To calculate the heat fluxes induced by mean currents and eddies, velocity and potential temperature are decomposed as $v=\bar{v}+v'$ and $\theta=\bar{\theta}+\theta'$, where the bar denotes monthly mean and the prime denotes deviation from there. Monthly average of equation (1) becomes,

$$c_p \rho \int_A \left(\bar{\theta}+\theta'-\theta_{ref}\right)\left(\bar{v}+v'\right) \mathrm{d}A = c_p \rho \int_A \left(\bar{\theta}-\theta_{ref}\right) \bar{v} \mathrm{d}A + c_p \rho \int_A \theta' v' \mathrm{d}A. \tag{2}$$

The first and second terms in equation (2) represent heat fluxes induced by mean currents and eddies, respectively. It is clear that the mean component depends on the reference temperature, unlike in the case of the eddy component. It means that the relative importance of heat fluxes by the mean currents and eddies depends on the choice of reference temperature. A detailed discussion of the relationship between the reference temperature and heat flux is made in the later section.

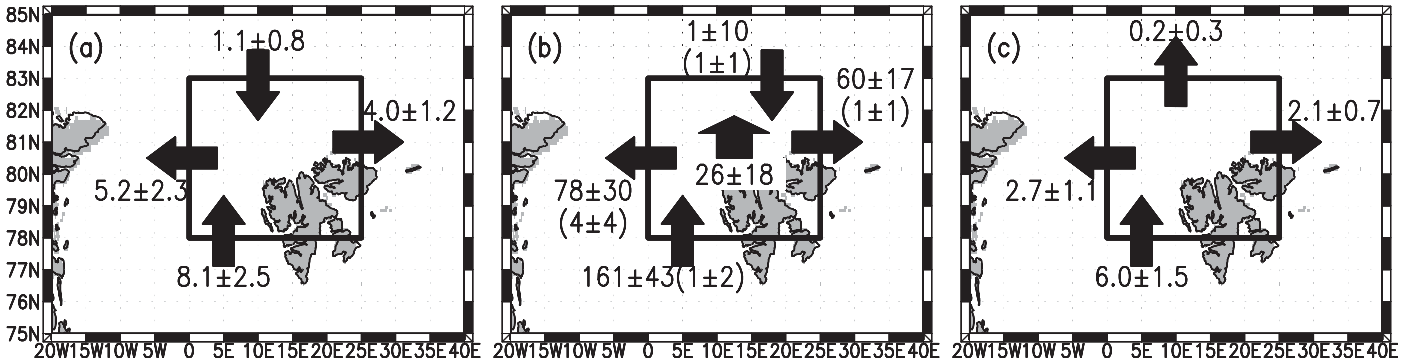

Figure 9. (a) Volume and (b) heat fluxes at each section (0–1000 m depth) in the north of the Fram Strait. Units are Sv (1 Sv = 10^6 m^3 s^{-1}) and TW (1 TW = 10^12 W), respectively. (c) Volume flux warmer than 2°C at each section (Sv). Value of heat flux in parentheses shows eddy-induced heat flux, and value following ± is standard deviation. The used reference temperature for calculation of heat flux is freezing point of seawater (−1.8°C).

Based on the above-described fine structures of currents to the north of the Fram Strait, a rectangular region indicated in Figure 6b is set, and heat flux is computed on each face. The relation between each section and current structure is summarized as follows (Figure 6b):

1. *Southern Section*: The northward transport of the Atlantic water by the WSC.
2. *Eastern Section*: The flux of the Atlantic water into the Nansen Basin (the Arctic Ocean interior) by the SVB and YPB.
3. *Western Section*: The westward transport of the Atlantic water provided by the WSC and YPB (after passing this section the water is transported southward by the EGC without flowing into the Arctic Ocean interior).
4. *Northern Section*: The southward flow of the Polar Water, which is part of anticlockwise boundary current in the Nansen Basin (after passing this section the water is transported eastward by the boundary current and passes through the eastern section).

The volume flux (0–1000 m depth) at each section is shown in Figure 9a. The bottom of box is defined as 1000 m depth, since the northward velocity core of WSC is limited to the shallower 1000 m depths (Figure 4b). The northward volume transport by the WSC is 8.1 Sv (1 Sv = 10^6 m^3 s^{-1}). 5.2 Sv (64%) of this water is transported westward and remaining 4.0 Sv (49%) is transported eastward. The volume transport at the eastern section, 4.0 Sv, is made up of the above mentioned eastward transport (2.9 Sv) and the Polar Water from the northern section (1.1 Sv). The vertical volume flux at 1000 m depth is negligible compared with that at horizontal sections. The volume transport at the sea surface, namely melting/freezing of sea ice, rain/snow fall, and evaporation, is also much smaller than the horizontal volume transport. On the other hand, the heat flux at the sea surface is significant and cannot be ignored as shown below.

The heat flux at each section is shown in Figure 9b. The northward heat transport by the WSC is 161 TW. 26 TW (16%) and 78 TW (48%) of this heat are removed by the sea surface cooling and westward transport, respectively. The remaining heat flux, 60 TW (37%), passes through the eastern section and is transported to the Arctic Ocean interior (the Nansen Basin). As the temperature of the Polar Water transported southward is low, the heat flux at the northern section (0.88 TW) is quite smaller than those at the other sections. Contribution of eddies is smaller than that of mean current at all sections, and the most significant contribution is found at the western section (4.7% of the total). Since high eddy activity is simulated in our model as in satellite observation, the smallness of eddy-induced heat transport is surprising. The contribution of eddies to heat flux is discussed in section 4.

The volume transport of water warmer than 2°C at each section is shown in Figure 9c. This definition of water is typical for the Atlantic water around the Fram Strait. The northward volume transport of the Atlantic Water is 6.0 Sv, 2.7 Sv (45%), and 2.1 Sv (35%) of this Atlantic Water are transported across the western and eastern sections, respectively. The Atlantic Water transport at the northern section is negligible (0.2 Sv). It is interesting that the fraction of Atlantic water volume transport across the eastern and western sections is same as those of whole volume and heat transports (westward transport is 1.3 times of eastward transport).

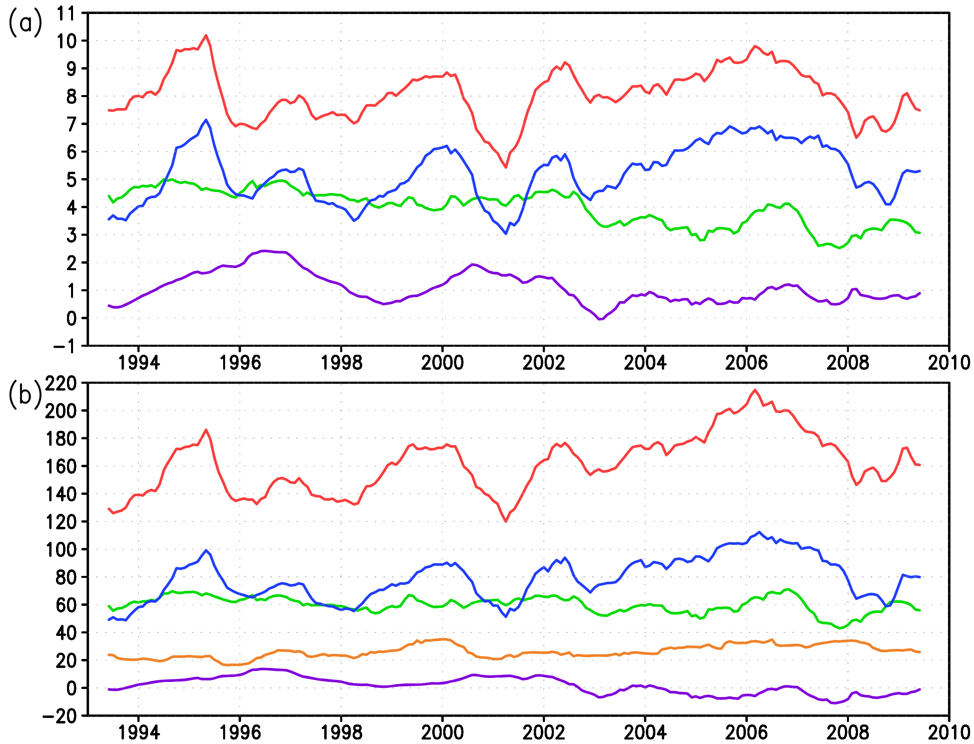

Figure 10. Time series of annual running mean of (a) volume flux and (b) heat flux at each section shown in Figure 9 (in Sv and TW, respectively). The used reference temperature for calculation of heat flux is freezing point of seawater (−1.8°C). Sign of value is consistent with arrow direction in Figure 9. Red, green, blue, purple, and orange lines indicate fluxes at the southern, eastern, western, northern sections, and sea surface.

To identify the factors controlling the interannual variability of the heat transports, the time series of heat flux at each section is shown in Figure 10b. The amount of heat transported westward (blue line) interannually varies similarly to the northward heat transport (red line) at 78°N (coefficient of correlation $r = 0.96$ with no lag). While the fluctuation range is small, the heat flux at the sea surface (orange line) has a high correlation with the northward heat flux at 78°N ($r = 0.68$). On the other hand, the eastward heat transport has low correlations with them ($r=0.06$). This result implies that the causes of the interannual variabilities of heat fluxes at the southern and western sections and sea surface are different from that at the eastern section.

The interannual variability of volume transport at each section is similar to that of heat flux (Figure 10a). A high correlation ($r = 0.85$) is found between the interannual variabilities of volume fluxes at the southern and western sections, although the correlations are low between the volume flux at the eastern section and those at the other sections (for instance, the correlation coefficient $r = -0.03$ between the volume fluxes at the southern and eastern sections). The correlation between the interannual variabilities of the volume and heat fluxes at each section is high ($r=0.84$, 0.96, 0.80, and 0.87 at the southern, western, eastern, and northern sections, respectively). This result suggests that the interannual variability of heat flux is associated with that of volume flux (current field).

Regression of the sea level pressure (SLP), which is dynamically linked to the near surface velocity field, onto the heat fluxes is taken. Here the 3 monthly mean value in winter (December–February), when the heat flux takes the maximum and the interannual variability is larger than in the other seasons, is utilized for the regression analysis. The correlation coefficients between annual and winter means of heat fluxes are 0.78 and 0.77 at the southern and eastern sections, respectively. Therefore, we can regard that the interannual variability of winter mean characterizes that of annual mean. Note that no statistical significance is found when the sea surface heat flux is regressed.

The distributions of the regression coefficient of the SLP on the heat fluxes at the southern and western sections and the sea surface have similar patterns (Figures 11a–11c). However, the distribution of the regression of the SLP on the heat flux at the eastern section differs from them (Figure 11d). The regressions of the

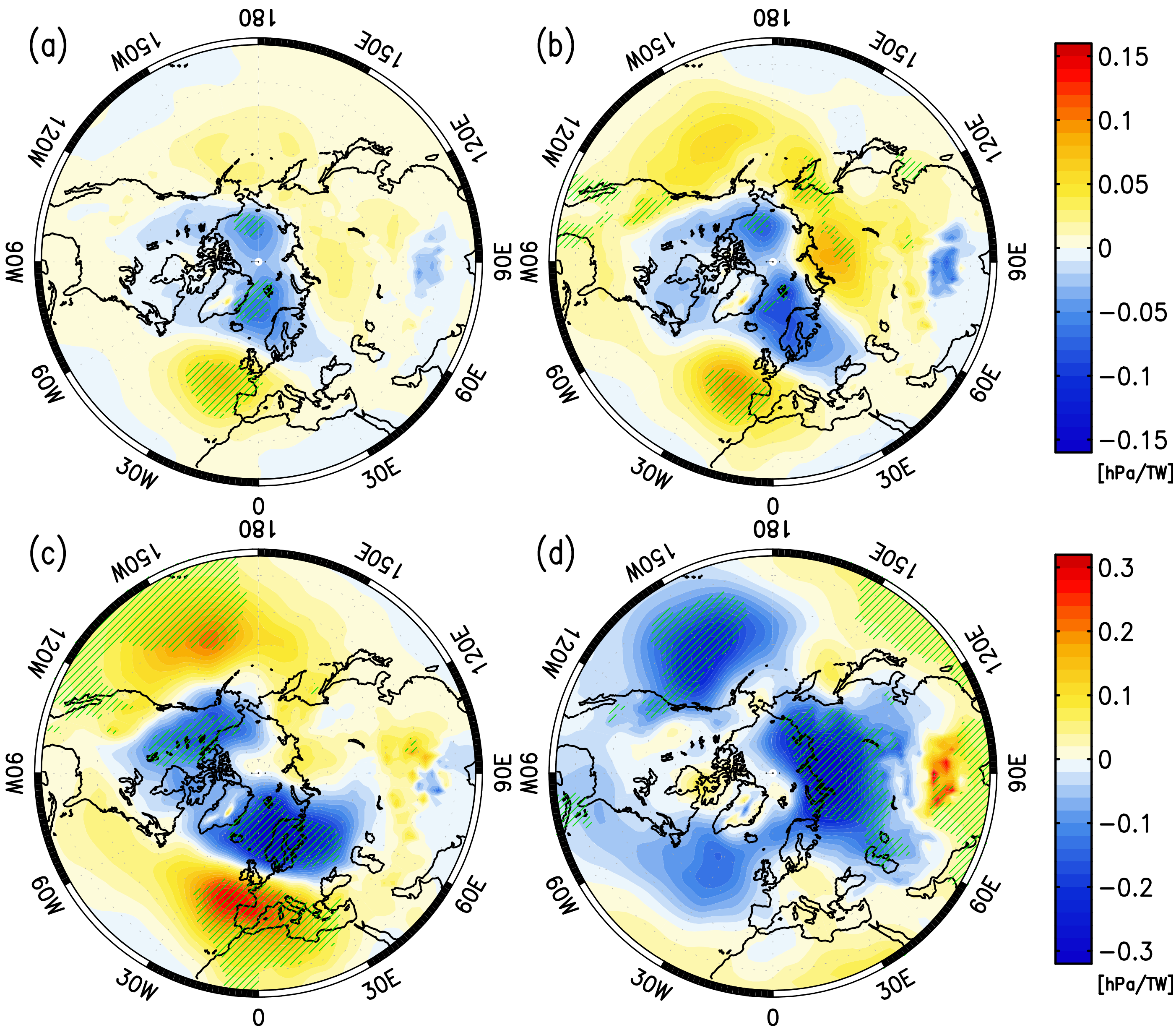

Figure 11. Distribution of winter (December–February; DJF) sea level pressure regressed onto heat flux at (a) southern, (b) western sections, (c) sea surface, and (d) eastern section (hPa TW^{-1}). Green hatch indicates high-correlation region exceeding the 90% of significant level.

SLP on the heat fluxes at the southern and western sections have a signal of low pressure centered at the Nordic Seas. It is shown that the enhancement/weakening of the low pressure induces the enhancement/weakening of the cyclonic circulation in the Nordic Seas and the increase/decrease of the volume and heat fluxes at the southern and western sections (Figures 11a and 11b). The region of high interannual variability in sea surface heat flux corresponds to the marginal ice zone (figure not shown). Thus, an anomalous low/high pressure centered at the Nordic Seas induces a shift of the sea-ice margin by the easterly/westerly wind anomaly and the enhancement/weakening of sea surface cooling in the region (Figure 11c).

Figures 11a–11c exhibit patterns similar to the North Atlantic Oscillation (NAO) [*Hurrell*, 1995]. The correlation coefficients between the NAO index and heat fluxes at the southern section and sea surface are 0.49 and 0.61 (both values exceed 95% significance level), respectively, for the period 1993–2009. *Blindheim et al.* [2000] and *Dickson et al.* [2000] demonstrated that the correlation between the 3 year running means of the winter NAO index and the observed temperature of the WSC around 76°N at 50–500 m depth is significantly high ($r = 0.8$).

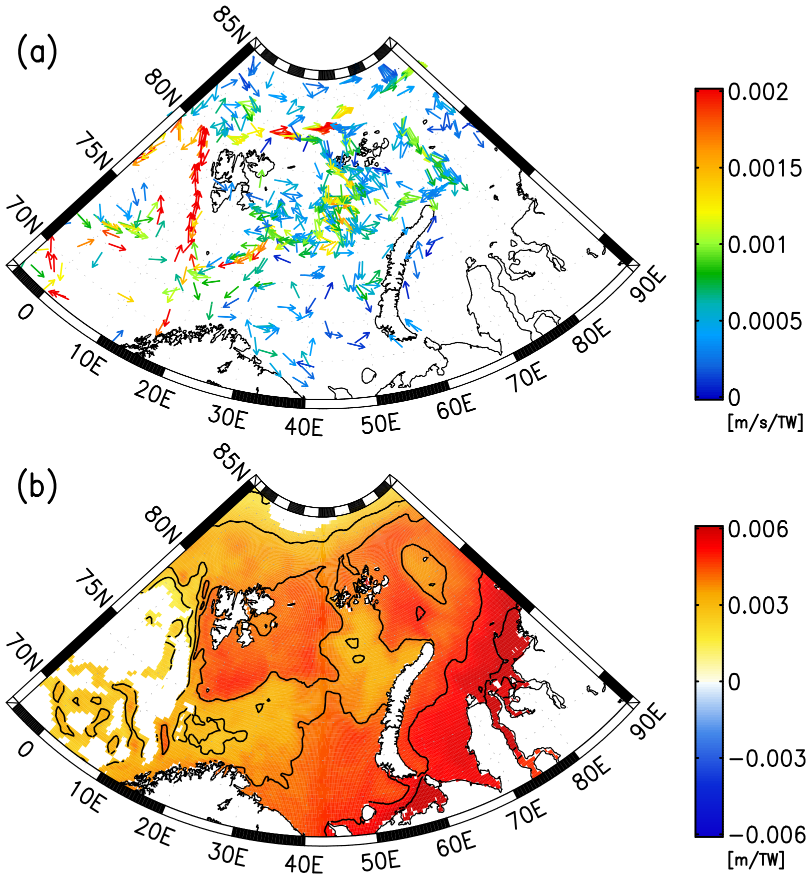

Figure 12. Distribution of regression coefficient of (a) horizontal velocity at 150 m depth and (b) sea surface height onto heat flux at the eastern section in winter (DJF). Units are m s^{-1} TW^{-1} and m TW^{-1}, respectively. Vector and shade are plotted only if correlation exceeds 90% significant level.

Saloranta and Haugan [2001] found the high correlation ($r = 0.79$) between the NAO and the observed temperature at around 79°N for the period 1975–1994 (95% significance level), although that for 1970–1994 is small ($r = 0.4$). Our study clarifies that the interannual variability of heat flux at 79°N is caused by the interannual variability of atmospheric pressure field, and this result is consistent with previous observational studies.

Saloranta and Haugan [2001] examined the variability of the observed temperature to the north of 79°N and in the region where the SVB and YPB flow. They have not presented the correlation with the NAO index probably because of the small number of the stations samples. The regression of the SLP to the heat flux at the eastern section, which corresponds to the region where *Saloranta and Haugan* [2001] examined the temperature variability, does not have the same pattern as the NAO in this study (Figure 11d). It rather corresponds to a negative anomaly of the Siberian high. The Siberian high is developed at the northeastern Eurasia in winter, and its enhancement induces decadal scale regime shifts of the central Arctic wind-driven circulation and sea-ice motion [*Proshutinsky and Johnson*, 1997]. The regression of the horizontal velocity field around the Barents Sea and the Fram Strait on the heat flux at the eastern section is shown in Figure 12a. This figure indicates that the enhancement/weakening of inflow of the Atlantic water through the Fram Strait is accompanied by the weakening/enhancement of the Atlantic water inflow through the Barents Sea. The regression of the sea surface height on the heat flux at the eastern section (Figure 12b) shows a high anomaly around the Svalbard and Framz-Josef Land, which is related to the anomalous circulation centered around this region (Figure 12a). In summary, the weakening/enhancement of Siberian high induces the northeasterly/southwesterly wind anomaly. This anomalous wind associates the anomalies of the sea surface height and circulation around the Svalbard and Framz-Josef Land by the Ekman transport. In consequence of this, decrease/increase of the inflow of the Atlantic water toward the Barents Sea accompanies the increase/decrease of the volume and heat fluxes at the north of the Fram Strait, namely the eastern section.

A previous modeling study demonstrated the negative correlation between the volume fluxes through the BSO and the Fram Strait caused by the same mechanism as in this study [*Lien et al*., 2013]. They presented it from data for just 2 years and explained the cause of the seasonal scale SLP variability is the meridional shift of the storm track related to the variability of the NAO. Our study is the first to show the negatively correlated variability between the inflows of the Atlantic water through the BSO and the Fram Strait associated with the variability of the Siberian high for the interannual time scale.

4. Discussion and Conclusions

The heat fluxes around the Fram Strait and causes of their interannual variabilities are examined by using an ice-ocean general circulation model, whose horizontal resolution is high (grid size $\sim$2–3 km) around the Fram Strait and the BSO. Our model reproduces the inflow of the Atlantic water toward the Arctic Ocean through the Fram Strait and the Barents Sea. The warm Atlantic water in the subsurface layer, which is kept apart from the sea surface cooling, enters the Arctic Ocean interior through the Fram Strait, whereas the heat transported by the Atlantic water is lost by the sea surface cooling in the Barents Sea. The simulated routes of the Atlantic water and heat transport are consistent with the observed view. The warming trend of the Atlantic water over the period 1997–2010 at the Fram Strait (79°N) is simulated well. The Atlantic water passing through the Fram Strait bifurcates to form the SVB and the YPB at north of 79°N, and a part of the Atlantic water in the YPB is transported westward by a mean current along a fracture zone. These routes of the Atlantic water to the north of the Fram Strait agree with observations. Satellite-observed features of eddy activity around the Fram Strait are also well reproduced in our model. A part of the warm Atlantic water is transported westward by such eddies.

A quantitative analysis of the heat flux to the north of the Fram Strait (78°N) is conducted. Forty-eight percent of heat of the Atlantic water passing through the Fram Strait is transported westward, 16% is lost by sea surface cooling, and the rest (37%) is transported to the Arctic Ocean interior, namely the Nansen Basin. The contribution of eddy to the westward heat transport is 5% of the whole. The cause of the interannual variability of heat passing through the Fram Strait and transported westward is the enhancement or weakening of the cyclonic circulation associated with the variability of the low pressure centered at the Nordic Seas. The interannual variability of the sea surface heat flux is caused by the enhancement/weakening of the sea surface cooling induced by the shift of sea-ice margin. This shift of sea-ice margin is a consequence of the easterly/westerly wind anomaly, which is also associated with the same SLP variability pattern as in the case of the westward heat flux. These interannual variabilities of heat fluxes have significant correlations with the NAO. On the other hand, it is demonstrated that the interannual variability of heat entering the Arctic Ocean interior (the Nansen Basin) is induced by the decrease/increase of the volume flux of the Atlantic water in the Barents Sea which is related to the weakening/enhancement of the Siberian high.

It is important to select the reference temperature for calculation of heat flux, if the section is not closed and net volume transport is not zero. *Schauer and Beszczynska-Möller* [2009] avoided problem of reference temperature selection for the WSC heat flux calculation by employing the "stream tube concept." This concept introduces a parameter, the minimum temperature of the WSC, and calculates the minimum temperature of outflow water such that the net volume flux (influx plus outflux) of them becomes zero. We also employed this method for heat flux calculation and validated our model result. Additionally, we also calculated the heat flux by employing the freezing point of seawater (-1.8°C) as the reference temperature. Since the value calculated as such corresponds to the heat consumed to melt sea ice, it is a good choice to estimate the effect of the Atlantic water passing through the Fram Strait on the sea ice in the Arctic Ocean. If the mean temperature in the box shown in Figure 6b is utilized as the reference temperature, the value represents the required heat to raise the temperature in the box. Previous studies widely used -0.1°C as the reference temperature for calculation of the heat flux around the Arctic Ocean. This value is first employed by *Aagaard and Greisman* [1975] and corresponds to the mean temperature of the southward EGC at the Fram Strait. The heat flux evaluated in section 3.1 is based on this value to compare with such studies. When the reference temperature is set to a lower value, the variability of heat flux becomes more sensitive to the volume flux variability. Although we concluded that the interannual variability of the heat flux is mainly caused by that of the volume flux, it is valid only when the "heat" is considered from the standpoint of how much sea ice it can melt.

It is interesting that the interannual variability of heat transport toward the Nansen Basin (at the eastern section) is not correlated with heat transport of the WSC (at northern section). We demonstrated that heat transport at the eastern section is related to the circulation around the Svalbard and Franz-Josef Land. Since this circulation includes the northward transport at the southern section, it is no wonder that interannual variabilities of heat fluxes at southern and eastern sections are synchronous. The standard deviation of heat flux at the eastern section (17 TW) is significantly smaller than that at the southern section (43 TW) and the western section (30 TW) (Figure 9b). Thus, the interannual variability of heat flux induced by the enhancement/weakening of the cyclonic current centered at the Nordic Seas is significantly larger than that induced by the cyclonic current variability around the Svalbard and Franz-Josef Land. Consequently, the interannual variability of heat flux at the southern section is not so much induced by the Siberian high variability but mainly induced by the low pressure variability centered at the Nordic Seas related to the NAO.

We employed eddy-resolving resolution only around the Fram Strait and Barents Sea. Although the locally fine structure of currents and eddies can be simulated, the currents and eddies far from the Fram Strait (e.g., the Gulf Stream, Pacific water eddy-induced transport toward the Arctic Ocean) are not well reproduced in our model. The high-temperature bias ($+1^\circ$C) of the Atlantic water around the Fram Strait is caused by the poor representation of currents in the North Atlantic Ocean. The nudging of temperature and salinity is generally employed to avoid such model drift. However, the restoring to coarse climatology temperature and salinity for eddy-resolving simulations causes unphysical processes and decay of fine current structure and eddies. Because longer period integration could cause a larger drift of the simulated fields, we conducted an only 20 year free (without nudging of temperature and salinity) model run in this study. Therefore, for instance, the role of the Atlantic Multidecadal Oscillation, which is a $\sim$70 year cycle of North Atlantic SST [*Enfield et al.*, 2001], on the Atlantic water inflow through the Fram Strait cannot be studied by our model. The Pacific water inflow is also the factor of recent Arctic sea ice retreat [*Shimada et al.*, 2006]. The Pacific water transport from the Chukchi Sea to the Canada Basin (Arctic Ocean interior) is induced by mesoscale eddies [*Watanabe and Hasumi*, 2009]. Since such eddy activity is not reproduced in our model, the recent decline of the Arctic sea ice cannot be investigated in this study. A model of high resolution for the whole Arctic Ocean should be utilized for examining the effects of both Pacific and Atlantic waters on the Arctic sea ice.

We demonstrated that the interannual variability of heat flux toward the Nansen Basin is related to the Siberian high variability. The strengthen of Siberian high induces the weakening of Atlantic water inflow toward the Nansen Basin, and finally the sea ice in the Nansen Basin. Several recent studies showed that the Arctic sea ice retreat induces enhancement of winter Siberian high [*Inoue et al.*, 2012; *Tang et al.*, 2013; *Mori et al.*, 2014]. These studies suggested only the effect of the Arctic sea ice on the atmosphere (the Siberian high). Our study presented the first scientific evidence of possible effect of atmospheric (the Siberian high) change on the oceanic heat flux. The linked variability of the Arctic sea ice and Siberian high should be examined by using a climate model.

Acknowledgments
This work is supported by the MEXT/GRENE and MEXT/JSPS KAKENHI (26247080). Numerical calculations were performed on FX10 at Information Technology Center, University of Tokyo. Almost all figures are drawn by using the Grid Analysis and Display System (GrADS) developed by M. Doty and M. Fiorino. The bathymetry of model is constructed from a 2 min Gridded Global Relief Data (ETOPO2v2) at http://www.ngdc.noaa.gov/mgg/global/etopo2.html. The sea surface heat, freshwater, and momentum fluxes of ice-ocean model are calculated using the corrected interannual forcing data sets (ciaf) version 2.0 for common ocean-ice reference experiments at http://data1.gfdl.noaa.gov/nomads/forms/core/COREv2/CIAF_v2.html.

References

Aagaard, K., and P. Greisman (1975), Toward new mass and heat budgets for the Arctic Ocean, *J. Geophys. Res.*, *80*(27), 3821–3827.
Aagaard, K., A. Foldvik, and S. R. Hillman (1987), The West Spitsbergen Current: Disposition and water mass transformation, *J. Geophys. Res.*, *92*(C4), 3778–3784.
Aagaard, K., et al. (1996), US, Canadian researchers explore Arctic Ocean, *Eos Trans. AGU*, *77*(22), 209–213.
Aksenov, Y., S. Bacon, A. C. Coward, and A. J. G. Nurser (2010), The North Atlantic inflow to the Arctic Ocean: High-resolution model study, *J. Mar. Syst.*, *79*(1), 1–22.
Aksenov, Y., V. V. Ivanov, A. J. Nurser, S. Bacon, I. V. Polyakov, A. C. Coward, A. C. Naveira-Garabato, and A. Beszczynska-Moeller (2011), The Arctic circumpolar boundary current, *J. Geophys. Res.*, *116*, C09017, doi:10.1029/2010JC006637.
Beszczynska-Möller, A., E. Fahrbach, U. Schauer, and E. Hansen (2012), Variability in Atlantic water temperature and transport at the entrance to the Arctic Ocean, 1997–2010, *ICES J. Mar. Sci.*, *69*, 852–863.
Bitz, C. M., and W. H. Lipscomb (1999), An energy-conserving thermodynamic model of sea ice, *J. Geophys. Res*, *104*(C7), 15,669–15,677.
Bitz, C. M., M. M. Holland, A. J. Weaver, and M. Eby (2001), Simulating the ice-thickness distribution in a coupled climate model, *J. Geophys. Res.*, *106*(C2), 2441–2463.
Blindheim, J., V. Borovkov, B. Hansen, S.-A. Malmberg, W. R. Turrell, and S. Østerhus (2000), Upper layer cooling and freshening in the Norwegian Sea in relation to atmospheric forcing, *Deep Sea Res., Part I*, *47*(4), 655–680.
Bourke, R. H., A. M. Weigel, and R. G. Paquette (1988), The westward turning branch of the West Spitsbergen Current, *J. Geophys. Res.*, *93*(C11), 14,065–14,077.
Carmack, E. C., R. W. Macdonald, R. G. Perkin, F. A. McLaughlin, and R. J. Pearson (1995), Evidence for warming of Atlantic water in the Southern Canadian Basin of the Arctic Ocean: Results from the Larsen-93 Expedition, *Geophys. Res. Lett.*, *22*(9), 1061–1064.
Cokelet, E. D., N. Tervalon, and J. G. Bellingham (2008), Hydrography of the West Spitsbergen Current, Svalbard Branch: Autumn 2001, *J. Geophys. Res.*, *113*, C01006, doi:10.1029/2007JC004150.
Comiso, J. C., C. L. Parkinson, R. Gersten, and L. Stock (2008), Accelerated decline in the Arctic sea ice cover, *Geophys. Res. Lett.*, *35*, L01703, doi:10.1029/2007GL031972.
Dickson, R. R., T. J. Osborn, J. W. Hurrell, J. Meincke, J. Blindheim, B. Adlandsvik, T. Vinje, G. Alekseev, and W. Maslowski (2000), The Arctic ocean response to the North Atlantic oscillation, *J. Clim.*, *13*(15), 2671–2696.

Dmitrenko, I. A., I. V. Polyakov, S. A. Kirillov, L. A. Timokhov, I. E. Frolov, V. T. Sokolov, H. L. Simmons, V. V. Ivanov, and D. Walsh (2008), Toward a warmer Arctic Ocean: Spreading of the early 21st century Atlantic Water warm anomaly along the Eurasian Basin margins, *J. Geophys. Res.*, *113*, C05023, doi:10.1029/2007JC004158 .

Enfield, D., A. Mestas-Nunez, and P. Trimble (2001), The Atlantic multidecadal oscillation and its relation to rainfall and river flows in the continental U. S., *Geophys. Res. Lett.*, *28*(10), 2077–2080.

Fox-Kemper, B., and R. Ferrari (2008), Parameterization of mixed layer eddies. Part II: Prognosis and impact, *J. Phys. Oceanogr.*, *38*(6), 1166–1179.

Fox-Kemper, B., R. Ferrari, and R. Hallberg (2008), Parameterization of mixed layer eddies. Part I: Theory and diagnosis, *J. Phys. Oceanogr.*, *38*(6), 1145–1165.

Griffies, S. M., and R. W. Hallberg (2000), Biharmonic friction with a Smagorinsky-like viscosity for use in large-scale eddy-permitting ocean models, *Mon. Weather Rev.*, *128*(8), 2935–2946.

Hall, D. K., and G. A. Riggs (2015), *MODIS/Aqua Sea Ice Extent and IST Daily L3 Global 4 km EASE-Grid Day, Version 6*, NASA Natl. Snow and Ice Data Cent. Distrib. Active Arch. Cent., Boulder, Colo., doi:10.5067/MODIS/MYD29E1D.006.

Hasumi, H. (2006), *CCSR Ocean Component Model (COCO) Version 4.0*, vol. 25, Cent. for Clim. Syst. Res., Univ. of Tokyo, Tokyo.

Hunke, E. C., and J. K. Dukowicz (1997), An elastic-viscous-plastic model for sea ice dynamics, *J. Phys. Oceanogr.*, *27*(9), 1849–1867.

Hurrell, J. (1995), Decadal trends in the North Atlantic Oscillation: Regional temperatures and precipitation, *Science*, *269*(5224), 676–679.

Inoue, J., M. Hori, and K. Takaya (2012), The role of Barents Sea ice in the wintertime cyclone track and emergence of a warm-Arctic cold-Siberian anomaly, *J. Clim.*, *25*(7), 2561–2568.

Johannessen, J. A., et al. (1987), Mesoscale eddies in the Fram Strait marginal ice zone during the 1983 and 1984 Marginal Ice Zone Experiments, *J. Geophys. Res.*, *92*(C7), 6754–6772.

Johannessen, O. M., H. Sagen, S. Sandven, and K. V. Stark (2003), Hotspots in ambient noise caused by ice-edge eddies in the Greenland and Barents Seas, *IEEE J. Oceanic Eng.*, *28*(2), 212–228.

Kawasaki, T., and H. Hasumi (2014), Effect of freshwater from the West Greenland Current on the winter deep convection in the Labrador Sea, *Ocean Modell.*, *75*, 51–64.

Komuro, Y., and T. Suzuki (2013), Impact of subgrid-scale ice thickness distribution on heat flux on and through sea ice, *Ocean Modell.*, *71*, 13–25.

Large, W. G., and S. G. Yeager (2009), The global climatology of an interannually varying air-sea flux data set, *Clim. Dyn.*, *33*(2–3), 341–364.

Lien, V. S., F. B. Vikebø, and Ø. Skagseth (2013), One mechanism contributing to co-variability of the Atlantic inflow branches to the Arctic, *Nat. Comm.*, *4*, 1488.

Lipscomb, W. H. (2001), Remapping the thickness distribution in sea ice models, *J. Geophys. Res.*, *106*(C7), 13,989–14,000.

Lique, C. (2015), Ocean science: Arctic sea ice heated from below, *Nat. Geosci.*, *8*, 172–173.

Maslowski, W., D. Marble, W. Walczowski, U. Schauer, J. L. Clement, and A. J. Semtner (2004), On climatological mass, heat, and salt transports through the Barents Sea and Fram Strait from a pan-Arctic coupled ice-ocean model simulation, *J. Geophys. Res.*, *109*, C03032, doi:10.1029/2001JC001039.

Mori, M., M. Watanabe, H. Shiogama, J. Inoue, and M. Kimoto (2014), Robust Arctic sea-ice influence on the frequent Eurasian cold winters in past decades, *Nat. Geosci.*, *7*, 869–873.

NASA Goddard Space Flight Center (2014), *Modis-Aqua Ocean Color Data*, NASA Goddard Space Flight Cent., Ocean Ecol. Lab., Ocean Biol. Process. Group, Greenbelt, Md., doi:10.5067/AQUA/MODIS_OC.2014.0.

National Geophysical Data Center (2006), National Oceanic and Atmospheric Administration, ETOPO2v2 Global Gridded 2-minute Database, Boulder, Colo. [Available at http://www.ngdc.noaa.gov/mgg/global/etopo2.html.]

Polyakov, I. V., et al. (2010), Arctic Ocean warming contributes to reduced polar ice cap, *J. Phys. Oceanogr.*, *40*(12), 2743–2756.

Polyakov, I. V., A. Pnyushkov, R. Rember, V. Ivanov, Y. Lenn, L. Padman, and E. Carmack (2012), Mooring-based observations of double-diffusive staircases over the Laptev Sea slope, *J. Phys. Oceanogr.*, *42*(1), 95–109.

Prather, M. J. (1986), Numerical advection by conservation of second-order moments, *J. Geophys. Res.*, *91*(D6), 6671–6681.

Proshutinsky, A. Y., and M. A. Johnson (1997), Two circulation regimes of the wind-driven Arctic Ocean, *J. Geophys. Res.*, *102*(C6), 12,493–12,514.

Quadfasel, D., J.-C. Gascard, and K. P. Koltermann (1987), Large-scale oceanography in Fram Strait during the 1984 Marginal Ice Zone Experiment, *J. Geophys. Res.*, *92*(C7), 6719–6728.

Rainville, L., and P. Winsor (2008), Mixing across the Arctic Ocean: Microstructure observations during the Beringia 2005 expedition, *Geophys. Res. Lett.*, *35*, L08606, doi:10.1029/2008GL033532.

Rippeth, T., B. Lincoln, Y. Lenn, J. Green, A. Sundfjord, and S. Bacon (2015), Tide-mediated warming of Arctic halocline by Atlantic heat fluxes over rough topography, *Nat. Geosci.*, *8*, 191–194.

Rothrock, D. A., Y. Yu, and G. A. Maykut (1999), Thinning of the Arctic sea-ice cover, *Geophys. Res. Lett.*, *26*(23), 3469–3472.

Rothrock, D. A., D. B. Percival, and M. Wensnahan (2008), The decline in Arctic sea-ice thickness: Separating the spatial, annual, and interannual variability in a quarter century of submarine data, *J. Geophys. Res.*, *113*, C05003, doi:10.1029/2007JC004252.

Rudels, B., R. Meyer, E. Fahrbach, V. V. Ivanov, S. Østerhus, D. Quadfasel, U. Schauer, V. Tverberg, and R. A. Woodgate (2000), Water mass distribution in Fram Strait and over the Yermak Plateau in summer 1997, in *Annales Geophysicae*, edited by European Geosciences Union (EGU), vol. 18, pp. 687–705, Springer, Berlin-Heidelberger, Germany.

Rudels, B., G. Björk, J. Nilsson, P. Winsor, I. Lake, and C. Nohr (2005), The interaction between waters from the Arctic Ocean and the Nordic Seas north of Fram Strait and along the East Greenland Current: Results from the Arctic Ocean-02 Oden expedition, *J. Mar. Syst.*, *55*(1), 1–30.

Saloranta, T. M., and P. M. Haugan (2001), Interannual variability in the hydrography of Atlantic water northwest of Svalbard, *J. Geophys. Res.*, *106*(C7), 13,931–13,943.

Schauer, U., and A. Beszczynska-Möller (2009), Problems with estimation and interpretation of oceanic heat transport-conceptual remarks for the case of Fram Strait in the Arctic Ocean, *Ocean Sci.*, *5*(4), 487–494.

Schauer, U., H. Loeng, B. Rudels, V. K. Ozhigin, and W. Dieck (2002), Atlantic water flow through the Barents and Kara Seas, *Deep Sea Res., Part I*, *49*(12), 2281–2298.

Schauer, U., E. Fahrbach, S. Osterhus, and G. Rohardt (2004), Arctic warming through the Fram Strait: Oceanic heat transport from 3 years of measurements, *J. Geophys. Res.*, *109*, C06026, doi:10.1029/2003JC001823.

Schauer, U., A. Beszczynska-Möller, W. Walczowski, E. Fahrbach, J. Piechura, and E. Hansen (2008), Variation of measured heat flow through the Fram Strait between 1997 and 2006, in *Arctic-Subarctic Ocean Fluxes*, edited by R. R. Dickson, J. Meincke, and P. Rhines, pp. 65–85, Springer, Dordrecht.

Screen, J. A., and I. Simmonds (2010), The central role of diminishing sea ice in recent Arctic temperature amplification, *Nature*, *464*(7293), 1334–1337.

Serreze, M. C., M. M. Holland, and J. Stroeve (2007), Perspectives on the Arctic's shrinking sea-ice cover, *Science*, *315*(5818), 1533–1536.
Shimada, K., F. McLaughlin, E. Carmack, A. Proshutinsky, S. Nishino, and M. Itoh (2004), Penetration of the 1990s warm temperature anomaly of Atlantic Water in the Canada Basin, *Geophys. Res. Lett.*, *31*, L20301, doi:10.1029/2004GL020860.
Shimada, K., T. Kamoshida, M. Itoh, S. Nishino, E. Carmack, F. McLaughlin, S. Zimmermann, and A. Proshutinsky (2006), Pacific Ocean inflow: Influence on catastrophic reduction of sea ice cover in the Arctic Ocean, *Geophys. Res. Lett.*, *33*, L08605, doi:10.1029/2005GL025624.
Skagseth, O., K. Drinkwater, and E. Terrile (2011), Wind-and buoyancy-induced transport of the Norwegian Coastal Current in the Barents Sea, *J. Geophys. Res.*, *116*, C08007, doi:10.1029/2011JC006996.
Smedsrud, L. H., R. Ingvaldsen, J. E. Ø. Nilsen, and Ø. Skagseth (2010), Heat in the Barents Sea: Transport, storage, and surface fluxes, *Ocean Sci.*, *6*, 219–234.
Steele, M., R. Morley, and W. Ermold (2001), PHC: A global ocean hydrography with a high quality Arctic Ocean, *J. Clim.*, *14*, 2079–2087.
Tang, Q., X. Zhang, X. Yang, and J. Francis (2013), Cold winter extremes in northern continents linked to Arctic sea ice loss, *Environ. Res. Lett.*, *8*(1), 014036.
Teigen, S. H., F. Nilsen, and B. Gjevik (2010), Barotropic instability in the West Spitsbergen Current, *J. Geophys. Res.*, *115*, C07016, doi:10.1029/2009JC005996.
Tsubouchi, T., et al. (2012), The Arctic Ocean in summer: A quasi-synoptic inverse estimate of boundary fluxes and water mass transformation, *J. Geophys. Res.*, *117*, C01024, doi:10.1029/2011JC007174.
Umlauf, L., and H. Burchard (2003), A generic length-scale equation for geophysical turbulence models, *J. Mar. Res.*, *61*(2), 235–265.
Walczowski, W. (2013), Frontal structures in the West Spitsbergen Current margins, *Ocean Sci.*, *9*, 957–975.
Walczowski, W., and J. Piechura (2006), New evidence of warming propagating toward the Arctic Ocean, *Geophys. Res. Lett.*, *33*, L12601, doi:10.1029/2006GL025872.
Watanabe, E., and H. Hasumi (2009), Pacific water transport in the western Arctic Ocean simulated by an eddy-resolving coupled sea ice-ocean model, *J. Phys. Oceanogr.*, *39*(9), 2194–2211.